Psychophysiology, 48 (2011), 1489–1498. Wiley Periodicals, Inc. Printed in the USA.

DOI: 10.1111/j.1469-8986.2011.01222.x

Perceptual reversals during binocular rivalry: ERP components and their concomitant source differences

JULIANE BRITZ[a] AND MICHAEL A. PITTS[b]

[a]Department of Fundamental Neuroscience and Geneva Neuroscience Center, University of Geneva, Geneva, Switzerland
[b]Department of Neurosciences, University of California, San Diego, San Diego, California, USA

Abstract

We used an intermittent stimulus presentation to investigate event-related potential (ERP) components associated with perceptual reversals during binocular rivalry. The combination of spatiotemporal ERP analysis with source imaging and statistical parametric mapping of the concomitant source differences yielded differences in three time windows: reversals showed increased activity in early visual (~120 ms) and in inferior frontal and anterior temporal areas (~ 400–600 ms) and decreased activity in the ventral stream (~250–350 ms). The combination of source imaging and statistical parametric mapping suggests that these differences were due to differences in generator strength and not generator configuration, unlike the initiation of reversals in right inferior parietal areas. These results are discussed within the context of the extensive network of brain areas that has been implicated in the initiation, implementation, and appraisal of bistable perceptual reversals.

Descriptors: Binocular rivalry, Perceptual reversal, Visual awareness, ERP

Multistable perception is a powerful vehicle to discern perceptual awareness from sensory processing. It occurs when ambiguous figures such as the Necker cube or Rubin's face–vase illusion have mutually exclusive interpretations or when binocular rivalry arises between dissimilar and thus incompatible images simultaneously presented to the two eyes (Sterzer, Kleinschmidt, & Rees, 2009). In both cases, perceptual awareness of physically identical stimuli alternates stochastically between two (or more) interpretations. For ambiguous figures, a single stimulus is presented to both eyes and perception switches (''reverses'') between each possible interpretation every few seconds. In contrast, binocular rivalry involves the simultaneous presentation of two different stimuli, one to each eye, and these stimuli compete for temporary perceptual dominance.

Binocular rivalry is likely to involve competition between stimuli and competition between percepts (Blake & Logothetis, 2002), each of which may occur at various stages along the visual stream. Previous research has primarily focused on identifying brain areas in which this competition is resolved (Tong, Meng, & Blake, 2006). To do so, most studies have compared brain activity associated with Percept A versus Percept B or activity associated with Percept A during rivalry versus Percept A during nonrivalrous (monocular) control conditions (Pitts, Martínez, & Hillyard, 2010b). Several functional magnetic resonance imaging (fMRI) studies in humans suggest that rivalry begins to be resolved in anatomically early visual areas, namely, the lateral geniculate nucleus and V1 (Haynes, Deichmann, & Rees, 2005; Lee, Blake, & Heeger, 2005; Polonsky, Blake, Braun, & Heeger, 2000; Wunderlich, Schneider, & Kastner, 2005) or extrastriate areas (Brouwer & van Ee, 2007; Haynes & Rees, 2005; Meng, Remus, & Tong, 2005; Tong, Nakayama, Vaughan, & Kanwisher, 1998). Single-cell recordings in nonhuman primates have shown that the currently active percept is strongly correlated with discharge rates in lateral occipital and inferior temporal regions and less so in early visual areas (Leopold & Logothetis, 1996, 1999; Logothetis, Leopold, & Sheinberg, 1996). Apart from visual areas, nonvisual areas in prefrontal and inferior parietal cortex have similarly been linked with subjective visual awareness for both ambiguous figures (Sterzer & Kleinschmidt, 2007; Sterzer, Russ, Preibisch, & Kleinschmidt, 2002) and binocular rivalry (Lumer, Friston, & Rees, 1998; Lumer & Rees, 1999).

In contrast to the breadth of research focusing on identifying brain activity correlated with each percept, much less is known about how the brain initiates, implements, and appraises the transitions between percepts. Perceptual reversals during binocular rivalry have received surprisingly little attention, and thus little is known about the neural systems involved. fMRI, because of its compromised temporal resolution, cannot disentangle

This work was supported by the National Institutes of Health (5 T32 MH20002, 2 R01 EY016984-35) and in part by the Swiss National Science Foundation (32003B-118315, 310030-132952), the Center for Biomedical Imaging (CIBM) of the Geneva and Lausanne Universities, EPFL, and the Leenaards and Louis-Jeantet foundations. The Cartool software (http://brainmapping.unige.ch/cartool) was programmed by Denis Brunet from the Functional Brain Mapping Laboratory, Geneva, Switzerland.

Address correspondence to: Juliane Britz, Ph.D., Department of Fundamental Neuroscience, Centre Médical Universitaire, 1, Rue Michel Servet, CH-1211 Genève 6, Switzerland. E-mail: juliane.britz@unige.ch

PSYCHOPHYSIOLOGY

which areas are linked with generating, executing, and evaluating perceptual changes during rivalry. The electroencephalogram (EEG), on the other hand, affords excellent temporal resolution, and the use of an intermittent stimulus presentation allows the precise time-locking of EEG events with stimulus onset. The EEG thus enables measurements that can help distinguish the processes related to the initiation, implementation, and appraisal of perceptual change during rivalry. The initiation of perceptual reversals refers to stimulus-independent intrinsic biases toward an upcoming perceptual change, whereas implementation denotes stimulus-dependent perceptual processes that underlie the perceptual change itself. The appraisal of reversals refers to the resultant cognitive evaluation of perceptual changes and what those changes mean for behavior.

Numerous studies have used an intermittent stimulus presentation to evaluate the stages of processing associated with perceptual reversals for various types of ambiguous figures (Britz, Landis, & Michel, 2009; Kornmeier & Bach, 2004, 2005, 2006; Pitts, Gavin, & Nerger, 2008; Pitts, Martínez, Brewer, & Hillyard, 2010a; Pitts, Martínez, Stalmaster, Nerger, & Hillyard, 2009; Pitts, Nerger, & Davis, 2007). These studies have revealed distinct event-related potential (ERP) components linked with perceptual reversals: an occipital negativity at ~250 ms (reversal negativity [RN]) followed by a parietal positivity after ~380 ms (late positive component [LPC], a P3b-like wave). In some studies, an early occipital positivity at ~120 ms (reversal positivity [RP]) has also been reported (Britz et al., 2009; Kornmeier & Bach, 2005, 2006; Pitts et al., 2007). Intracranial generators of two of these ERP components (the RN and the LPC) have been estimated using both a local autoregressive average (the LAURA inverse solution; Grave de Peralta Menendez, Murray, Michel, Martuzzi, & Gonzalez Andino, 2004) and current dipole modeling. Both methods suggested that the RN is generated in right occipital-temporal/fusiform gyrus regions, whereas the LPC is generated in bilateral anterior temporal and superior parietal regions (Pitts et al., 2009).

In addition to these stimulus-evoked ERP components (RP, RN, LPC) that are most likely associated with the implementation and appraisal of perceptual reversals, Britz et al. (2009) used an electrical neuroimaging approach (Michel, Koenig, Brandeis, Gianotti, & Wackermann, 2009; Murray, Brunet, & Michel, 2008) and identified a prestimulus EEG topography that reflected the initiation of Necker cube reversals. In the 50 ms prior to a reversal, activity increased in right inferior parietal regions. Recently, this finding was replicated for perceptual reversals during binocular rivalry (Britz, Pitts, & Michel, 2010).

Although this previous work has begun to elucidate the stages of processing associated with perceptual reversals of ambiguous figures and has started to draw links between ambiguous figures and rivalry, it remains unclear whether the same or different ERP components are associated with reversals of ambiguous figures and binocular rivalry. In the present study, we used electrical neuroimaging to explore the temporal dynamics of spontaneous perceptual alternations during binocular rivalry using an intermittent stimulus presentation. We investigated the time course of ERP scalp topographies and their concomitant intracranial generators for perceptual reversals and perceptual stability.

In addition to determining whether binocular rivalry reversals elicit the same ERP components as ambiguous figure reversals, this type of analysis allowed a more in-depth look at the generators of the reversal-related ERP components. Although previous studies (Pitts et al., 2009) had localized the sources of the RN and LPC difference wave components, it was unclear whether activity in these areas was enhanced or suppressed during reversals (compared to stability). Here, by conducting statistical parametric mapping of the sources for each ERP, we were able to assess which brain regions may be more or less active during perceptual reversals compared to perceptual stability.

Methods

The raw data used in this study are the same as those used by Britz et al. (2010) and Pitts, Martínez, and Hillyard (2010b). In Britz et al. (2010), we investigated the initiation of perceptual reversals by means of the prestimulus EEG microstate and its concomitant generator, and in Pitts, Martínez, and Hillyard (2010b), poststimulus ERPs were compared according to the dominant percept on each trial (Percept A vs. Percept B). In the present study, we investigated poststimulus activity associated with perceptual reversals (reversal vs. stable) by comparing the time course of stimulus-evoked microstates and their concomitant generators.

Participants

Fourteen healthy adults (8 female, mean age 20.29 years, range 18–23) participated in the experiment. One subject was excluded from the analyses because of substantial contamination by artifacts, and the data of 13 subjects were submitted to subsequent analyses. All subjects had normal or corrected-to normal visual acuity and no history of psychiatric or neurological impairments. Subjects were recruited as volunteers and gave informed consent prior to each experiment, and all experimental procedures were approved by the University of California at San Diego Institutional Review Board.

Stimuli and Procedure

Stimuli were square-shaped sinusoidal gratings subtending 6° of visual angle in diameter and were presented as pairs, one to each eye. The pairs were orthogonal on three dimensions: color (red vs. green), orientation (45° vs. 135°) and spatial frequency (1 cpd vs. 5 cpd) in order to minimize piecemeal rivalry. Including the factor eye (left vs. right), this yielded eight different pairs of stimuli. Each pair was equated in luminance by chromatic photometry and was presented in six nonconsecutive blocks of trials (counterbalanced across blocks), yielding 48 blocks. During each block, stimuli were presented 50 times (~1 min), and subjects took self-paced breaks between blocks. All stimuli were presented intermittently for 600 ms, and the interstimulus interval varied randomly between 500 and 700 ms. For each stimulus, participants were asked to indicate the color of their percept by means of a button press. They were instructed to withhold their response in case they perceived a piecemeal mixture between the two stimuli.

All stimuli were presented on a black background and centered horizontally within the left and right halves of a CRT computer screen with a refresh rate of 60 Hz. Participants viewed the stimuli through a mirror stereoscope, which allows the separate stimulation of the left and right eyes, and they adjusted the angle of the mirrors to achieve stereo fusion. A fixation cross (1°) was presented in the center of a gray/white circle (0.75°) to help

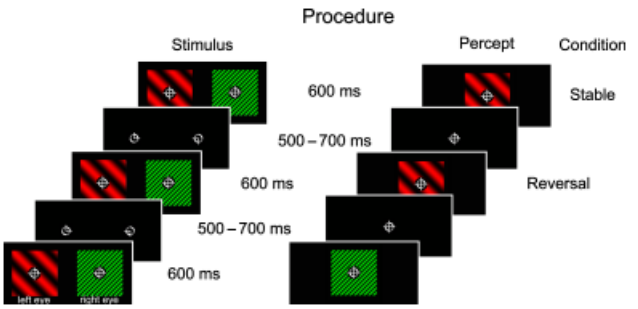

Figure 1. Stimuli and task. Subjects viewed monocular pairs of Gabor gratings orthogonal in color, orientation, and spatial frequency and indicated the color of their percepts via button presses. Stimuli were presented for 600 ms followed by a blank screen for 500–700 ms.

maintain fusion, and all stimuli were presented at fixation. Figure 1 depicts the stimuli and experimental procedure.

Prior to the ERP experiment, we behaviorally titrated the optimal durations for both stimulus presentation and the interstimulus intervals in order to mimic natural (continuous) reversal conditions. The optimal timing was chosen such that the stimulus presentation was long enough to ensure a clear percept (red or green) and to avoid the occurrence of perceptual reversals during the presentation. This was based on evidence from previous studies that have shown that orthogonal gratings can fuse into plaids if they are presented for less than 150 ms (Wolfe, 1983) and that perceptual alternations are prevented when the blank interval is extended to several seconds (Leopold, Wilke, Maier, & Logothetis, 2002; Sterzer & Rees, 2008).

EEG Acquisition and Raw Data Processing

The EEG was recorded from 64 tin electrodes mounted in an elastic cap (Electrocap International, Inc.), bandpass filtered between 0.1 and 80 Hz, continuously digitized at 250 Hz, and amplified with a battery-powered amplifier (SA Instrumentation) with a gain of 10,000. Impedances were kept below 5 kΩ, and the EEG was referenced online to the right mastoid. Horizontal and vertical eye movements were monitored with a bilateral external canthus montage and a suborbital electrode referenced to the right mastoid, respectively. Off-line, the EEG was recomputed to the common average reference.

For each stimulus, we determined whether perception alternated (reversal) or remained the same (stable) by comparing the current response with the response to the preceding stimulus, that is, when the response in trial n was different from trial $n-1$, this trial was classified as a reversal trial; when the responses in trial n and trial $n-1$ were the same, it was classified as a stable trial. Before segmenting the EEG data into epochs ranging from 100 ms before until 600 ms after stimulus onset, the ongoing EEG was bandpass filtered between 1 and 30 Hz using a second order Butterworth filter with a -12 db/octave rolloff. The filter was computed linearly with two passes (one forward and one backward), eliminating the phase shift, and with poles calculated each time to the desired cutoff frequency. Epochs contaminated by oculomotor and other artifacts as well as trials in which subjects experienced piecemeal rivalry were rejected. In a previous study (Britz et al., 2010), we found that perceptual reversals in the present setting arose as a consequence of increased right parietal activity immediately preceding perceptual reversals. We did not apply a baseline correction to the current data to prevent the prestimulus differences between the two conditions from appearing as poststimulus differences. The basics of the data-driven spatiotemporal analysis have been described elsewhere (Michel et al., 2004; Murray et al., 2008); here, we describe the processing steps in the section titled "Analysis of stimulus-evoked potentials". All EEG analyses were performed using the Cartool software by Denis Brunet (http://brainmapping.unige.ch/cartool).

Analysis of Behavioral Data and Statistical Properties of the Reversal Intervals

We computed the mean and median durations for the reversal intervals, that is, the time intervals between successive reversal trials, as well as the reaction times and the percentage of piecemeal rivalry. We previously confirmed that the intermittent stimulus presentation closely matched "natural" reversal conditions comparable to a continuous stimulus presentation by showing that the reversal intervals do not show any short-term correlations and that they follow a gamma and lognormal distribution (Britz et al., 2010) and that the intermittent stimulus presentation elicited reversal rates whose statistical properties are comparable to continuous stimulus presentations (Lehky, 1995).

Analysis of Stimulus-Evoked Potentials

We examined the stimulus-evoked differences between the reversal and stable conditions by using both global and local measures. The global measures assessed the time course of ERP topography modulations (Murray et al., 2008), and the local measures assessed the time course of ERP amplitude modulations.

First, we used a spatiotemporal segmentation procedure (Michel et al., 2004) to identify the periods of stable map topographies of the grand averaged ERPs in the reversal and stable conditions. This approach reveals whether the two conditions evoke the same potential fields under the two experimental conditions or not. It follows the notion that stimulus-evoked topography does not vary randomly but that it remains stable for discrete processing states with sharp transitions between states. Differences in topography necessarily imply different generators (Helmholtz, 1853; Vaughan, 1982), whereas the opposite is not necessarily true: Identical topographies can, in principle, be generated by different sources. We applied a spatial atomize-agglomerate hierarchical cluster analysis (AAHC; Murray et al., 2008) to identify the dominant clusters evoked in the reversal and stable conditions. We used a modified AAHC procedure such that we normalized the topographies with respect to the global field power (GFP), that is, we only considered the momentary topographic configuration irrespective of its overall strength.

We determined the optimal number of clusters and their corresponding template maps with a cross-validation criterion that is a measure of predictive residual variance as a function of the degrees of freedom, and its minimum is considered as the optimal number of clusters. Thus, the best solution of the cluster analysis is the one with maximal explained variance and minimal residual variance. Because map durations of less than 10 ms are physiologically implausible, we used an additional temporal constraint criterion of 10 ms. The cluster analysis was performed on both the reversal and stable conditions. This determined whether the same or different maps were evoked in the two conditions. We

then determined whether the template maps identified in the grand average could be identified in the individual subjects by computing a strength-independent spatial correlation between the series of template maps and the ERPs of every individual subject. We then assessed statistically whether the maps differed in terms of frequency of occurrence, GFP, and global explained variance (GEV) between the two conditions. The GFP is a measure of field strength and is equivalent to the spatial standard deviation of the scalp electrical field (Lehmann & Skrandies, 1980), and the GEV is the explained variance weighted by the GFP.

To compare our results with conventional ERP analysis approaches, we then examined amplitude modulations at each electrode by computing *t* tests between the reversal and stable conditions for each time point and each electrode. The *p* values were adjusted for multiple comparisons using a Sidak correction for multiple testing (Britz et al., 2010; Gonzalez Andino, Michel, Thut, Landis, & Grave de Peralta, 2005).

Analysis of Stimulus-Evoked Sources

We used a LORETA (Pascual-Marqui, Michel, & Lehmann, 1994) inverse solution to estimate the intracranial current distribution. LORETA was calculated in a simplified realistic head model (SMAC; Spinelli, Gonzalez Andino, Lantz, Seeck, & Michel, 2000): The average template brain of the Montreal Neurological Institute was used as the standard brain for all subjects. The brain surface was extracted from this MRI, and the best fitting sphere was estimated. Then the MRI was warped according to the ratio of the sphere radius and the real surface radius. Some 3005 solution points were then defined in regular distances within the gray matter of this standard brain. The forward problem was then solved with a three-layer conductor model using an analytical solution. Additional details can be found in Michel et al. (2004). The simplified realistic head model offers an easy and fast extraction of the head model and a fast and accurate analytical solution to the forward problem at the expense of being somewhat less precise than finite element models based on individual anatomy. Nevertheless, accurate source localization using this head model has been demonstrated in different clinical and experimental studies in the past (Groening et al., 2009; Lantz et al., 1997; Michel et al., 1999, 2004; Plomp, Michel, & Herzog, 2010; Schulz et al., 2008; Sperli et al., 2006; Vulliemoz et al., 2010; Zumsteg, Friedman, Wieser, & Wennberg, 2006). We computed the stimulus-evoked intracranial current distributions for the time periods in which ERP amplitudes differed between conditions and their corresponding topographies differed with respect to the GFP. We examined the sources for the periods of significant amplitude differences when they co-occurred with map strength differences.

Analysis of Stimulus-Evoked Source Differences

Because differences in topography always imply different generators, the interpretation of source images obtained from difference waves becomes problematic when amplitude differences arise from differences in topography: In that case, an amplitude difference wave does not reflect the spatial summation of the different underlying generators. Moreover, because intracranial source estimations can only be positive or zero (i.e., either there is source activity or there is none, but there cannot be negative activity), the sources of difference waves are blind to the direction of an effect, that is, they cannot reveal in which condition the intracranial current is larger. One way to overcome these problems is to assess the time course of statistical differences of the intracranial current sources (Britz & Michel, 2010; James, Britz, Vuilleumier, Hauert, & Michel, 2008; Plomp et al., 2010). Moreover, considering the time course of statistical differences instead of the source images themselves eliminates the problem of thresholding and so helps eliminate spurious sources of activity. Differences in intracranial generators can arise from differences in their configuration as well as from differences in their strength. Because identical scalp maps can arise from different generator configurations, identical scalp maps with different GFP may suggest but do not necessarily indicate identical generators with different strengths. One can disentangle the differential contributions of differences in generator configuration and generator strength by comparing the current density maps of the intracranial generators in two conditions on the one hand and the parametric map of their statistical difference on the other hand: If the generators of two conditions differ only with respect to their strength, their generator maps will be identical but differ in amplitude, and the magnitude of this difference will likewise be reflected in the statistical parametric map of their difference. In other words, if the scalp maps in two conditions are identical and if their difference map has the same topography, the generator maps will likely be identical for the two conditions, for the difference wave and for the statistical comparison between the two conditions. On the other hand, if the difference map is different from the maps in the two conditions, the source maps will likewise be different for the two conditions, the difference wave and the statistical comparison between the two conditions.

We estimated the intracranial current at each solution point for each time point for the reversal and stable conditions in each subject using the LORETA inverse solution described above. We then assessed the time course of statistical difference between the reversal and stable conditions by means of time-point-wise paired *t* tests at each solution point, an equivalent to statistical parametric mapping used in fMRI. Like for the amplitude analyses, we used a Sidak correction for multiple comparisons in addition to a temporal constraint criterion of 10 ms. We further assessed whether these statistical source differences were due to differences in generator strength or configuration by comparing the statistical parametric maps with current density maps of the corresponding time periods.

Figure 2. ERP surface and source results. A: Results of the temporal-spatial segmentation procedure. The temporal-spatial segmentation procedure yielded nine template maps, which are displayed in the middle panel. They are displayed with the left hemifield on the left and the nose on top. Red indicates positive polarity and blue negative polarity. The top and bottom panels depict the time course of the GFP for the reversal and stable conditions, respectively, and the color codes represent the presence of each map in the two conditions. B: Time course of ERP amplitude differences. ERP amplitudes differed in four time windows between reversal and stable conditions, their time course is shown in the plot (*p* values), and their location is illustrated by the maps (significant *t* values; positive differences in red, negative differences in blue). C: Time course of ERP source differences. ERP sources differed in virtually the same time windows as the amplitudes. Their time course is shown in the plot (*p* values), and their location is illustrated in the brains (*p* values) and *t* values. Positive *t* values are displayed in red–yellow colors and negative differences are displayed in blue–purple colors.

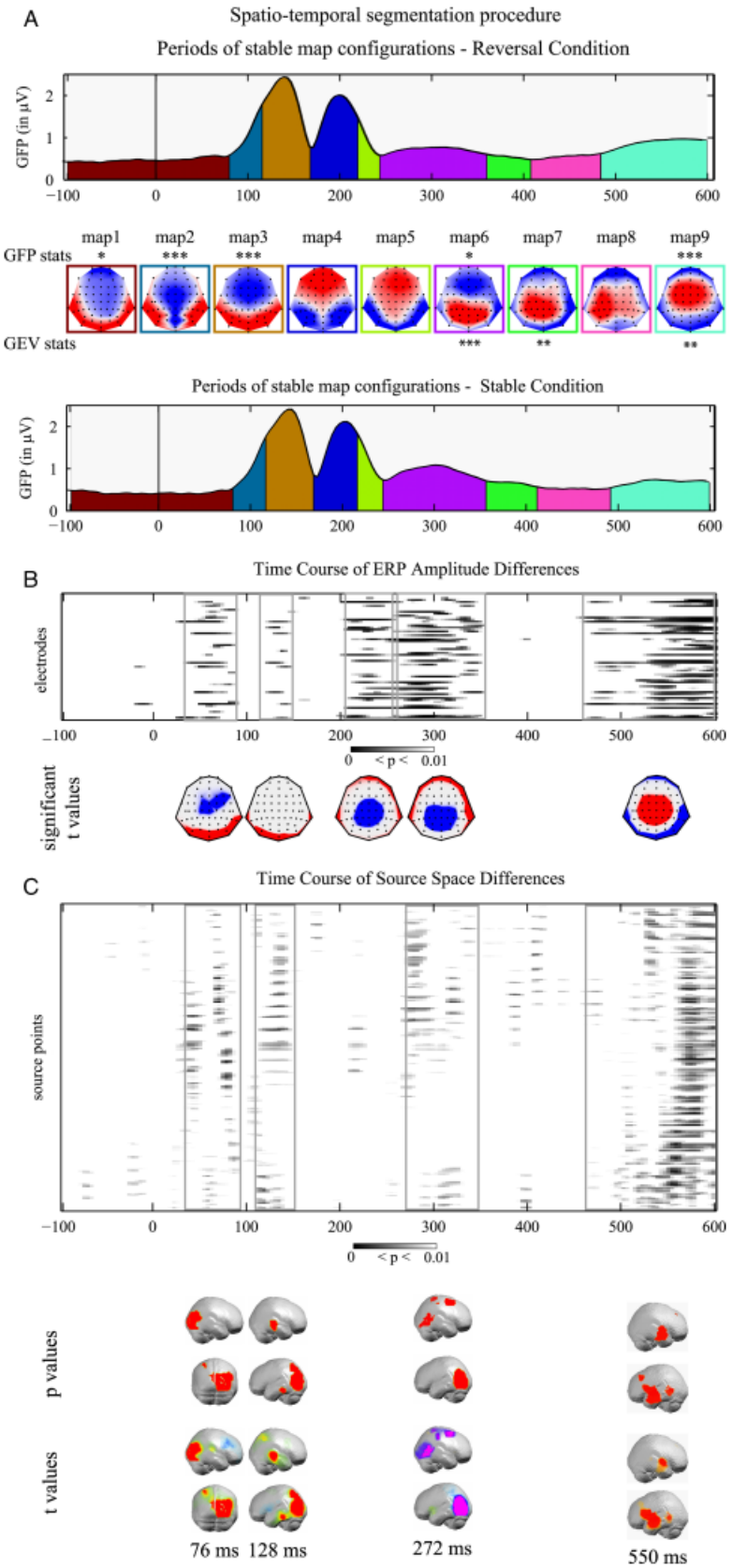
A
Spatio-temporal segmentation procedure
Periods of stable map configurations - Reversal Condition
GFP (in µV)
map1 map2 map3 map4 map5 map6 map7 map8 map9
GFP stats
GEV stats
Periods of stable map configurations - Stable Condition
B
Time Course of ERP Amplitude Differences
electrodes
0 < p < 0.01
significant t values
C
Time Course of Source Space Differences
source points
0 < p < 0.01
p values
t values
76 ms 128 ms
272 ms
550 ms

Table 1. *Periods of Occurrence (in Milliseconds) and Statistical Difference of Frequency of Occurrence, Global Explained Variance, and Global Field Power for Maps Identified in the Spatiotemporal Segmentation Procedure*

	Occurrence	Global explained variance			Global field power				
	Map 7	Map 6	Map 7	Map 9	Map 1	Map 2	Map 3	Map 6	Map 9
t value	3.56	− 4.367	− 3.16	3.56	2.72	4.38	5.25	− 2.79	3.96
p value	.004	.001	.009	.004	.019	.0001	.0003	.017	.0017

Results

Behavioral Results and Statistical Properties of the Reversal Intervals

The reversal intervals had a mean and median duration of 3052 and 2448 ms, respectively, and a standard deviation of 2080 ms, that is, perceptual reversals occurred, on average, every 3052 ms. The mean reaction time was 529 ms, and reactions were performed, on average, 609 ms before the onset of the next stimulus. On average, subjects experienced piecemeal rivalry in 3.1% of trials, and piecemeal rivalry never occurred in successive trials.

Stimulus-Evoked Potentials

Figure 2A shows the results of the spatiotemporal segmentation procedure. It yielded nine template potential maps, which explained 93.67% of the variance in the reversal and stable conditions. We assessed their statistical differences with respect to frequency of occurrence, global explained variance and global field power. These results are summarized in Table 1.

Conventional waveform analyses compared the amplitude difference between the reversal and stable conditions at each electrode and revealed significant amplitude differences in four time windows (Figure 2B). First, ERPs were more positive in the reversal than the stable condition in two time windows: 50–80 ms (Map 1) and 112–134 ms at occipital electrodes (RP; P1 component; Map 3). The first period of significant difference (50–80 ms) disappears when a prestimulus baseline correction is applied from − 100–0 ms (see Supplementary Figure 1). Next, ERPs were more negative in the reversal than the stable condition at centro-posterior electrodes from 200–350 ms (RN). The RN encompassed two ERP components, the N1 (200–250 ms; Map 5) and the P2 (250–350 ms; Map 6). Finally, ERPs were more positive in the reversal than the stable condition from 440 to 600 ms at centro-parietal electrodes (LPC; P3b component; Map 9). Figure 3 shows ERPs from two exemplar electrode sites to illustrate the waveforms of these components. The RP was the result of a more positive wave in the reversal than in the stable condition. The RN is the result of a more positive wave in the stable than in the reversal condition, and the LPC is the result of a more positive-going wave in the reversal than the stable condition.

To determine which of these amplitude differences reflected stimulus-related processing differences, we assessed when ERPs were significantly different from the baseline activity. To do so, we computed time-point-wise *t* tests between the poststimulus amplitude and a 200-ms prestimulus baseline. We found significant differences between the poststimulus ERPs and the baseline in four time windows: 100–150 ms, 180–224 ms, 272–392 ms, and 460–600 ms; that is, all amplitude differences except the earliest time window (50–80 ms) are the result of stimulus-related differences. Supplementary Figure 2 summarizes these results.

Stimulus-Evoked Sources

The intracranial current density maps for the time periods of significant amplitude differences are displayed in Figure 4A for the reversal and stable conditions and in Figure 4B for the corresponding difference waves.

The intracranial current distribution during the first significant difference (Map 1, 50–80 ms) was found in bilateral anterior cingulate and right anterior temporal regions, and it was larger for the reversal than the stable condition. The intracranial sources of the corresponding difference waves were found in bilateral middle temporal cortex and the left precentral gyrus. The intracranial sources during the RP (P1, Map 3, 110–140 ms) were found in bilateral lateral occipital areas and were larger in the stable than in the reversal condition, and the intracranial sources for the corresponding difference waves were virtually in the same areas. The intracranial sources during the RN (P2, Map 6, 240–350 ms) were found in bilateral lateral occipital cortex and were larger in the stable than in the reversal condition, and, for the corresponding difference wave, they were found in virtually the same lateral occipital areas and additionally in the right middle temporal cortex. The intracranial sources during the LPC (P3b, Map 9, 450–600 ms) were found in bilateral anterior temporal and inferior frontal areas and were larger in the reversal than in the stable condition, and those of the corresponding difference waves were found in the same inferior prefrontal and middle temporal areas as well as in lateral occipital cortex.

Stimulus-Evoked Source Differences

Significant differences in current density of the intracranial sources between the reversal and stable conditions occurred in four time windows (Figure 2C). The first differences were found in a time window ∼50–90 ms, during which sources were stronger in the reversal than in the stable condition in primary visual areas. The second time window corresponded to the RP (∼110–130 ms), and sources were stronger in the reversal than in the stable condition in lateral occipital areas and inferior temporal areas on the left and in middle temporal areas on the right. In the third time window, sources differed during the P2 period of the RN (∼250–300 ms). In this time window, sources were stronger in the stable than in the reversal condition in bilateral lateral occipital and right superior parietal areas. Finally, sources differed during the period of the LPC. In this time window (∼500–600 ms), sources were stronger in the reversal than in the stable condition in bilateral anterior temporal and left middle temporal and inferior frontal areas.

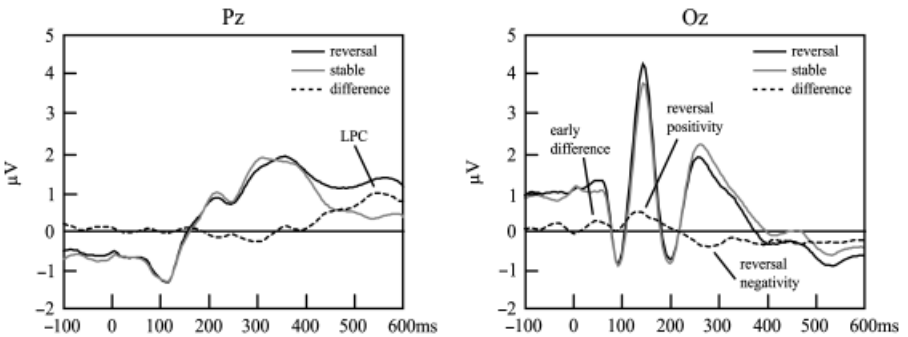

Figure 3. Exemplar ERP waveforms (average reference, not baseline corrected; see Methods section). ERPs are plotted for the reversal (black line) and stable (gray line) conditions and for the difference waves (dashed line; reversal minus stable) from two representative occipital/parietal electrode sites (Oz and Pz). Positive polarities are plotted up and negative polarities are plotted down. The earliest difference, the reversal positivity, and the reversal negativity can be seen at electrode Oz. The LPC can be seen at electrode Pz.

Discussion

We investigated the spatiotemporal dynamics of reversal-related ERPs and their concomitant intracranial generators during intermittent binocular rivalry. Conventional waveform analysis revealed that perceptual reversals during binocular rivalry elicit the same reversal-related ERP components that have been previously identified for ambiguous figures, namely, the RP, the RN, and the LPC (Britz et al., 2009; Kornmeier & Bach, 2004, 2005, 2006; Pitts et al., 2007, 2008, 2009). We assessed the time course of ERP surface differences with both global (topographic) and local (amplitude) measures on the one hand and the time course of their intracranial source differences based upon difference waves and time-point-wise statistics between conditions in the source space on the other hand. The latter was done to assess whether source differences were the result of modulations in strength of identical generators: If the intracranial sources of two conditions have the same distribution but with a different strength, and if the parametric map of their statistical comparison yields again the same distribution, this strongly suggests that they originate from the same intracranial generators that differ only in strength. The magnitude of the difference is reflected in the statistical parameters. If this is the case, the sources estimated from a difference wave distribution yield a valid result if they have the same distribution as the statistical parametric map. In this case, the scalp topography of the difference wave will be the same as the topography in either condition.

Based on these measures, the current analyses provide converging evidence suggesting that the implementation of perceptual reversals during binocular rivalry is indexed by a series of strength-based (as opposed to configuration-based) modulations of stimulus-dependent neural generators. Below, we discuss the results for each reversal-related component separately.

Reversal Positivity

Difference waves for perceptual reversals of ambiguous figures are usually computed by subtracting the ERPs of the stable condition from ERPs of the reversal condition; however, the direction of subtraction is rather arbitrary and may reflect unfounded assumptions that reversals are associated with increased neural activity. The topographic ERP analysis revealed that the RP is the result of differences in field strength of the P1 com-

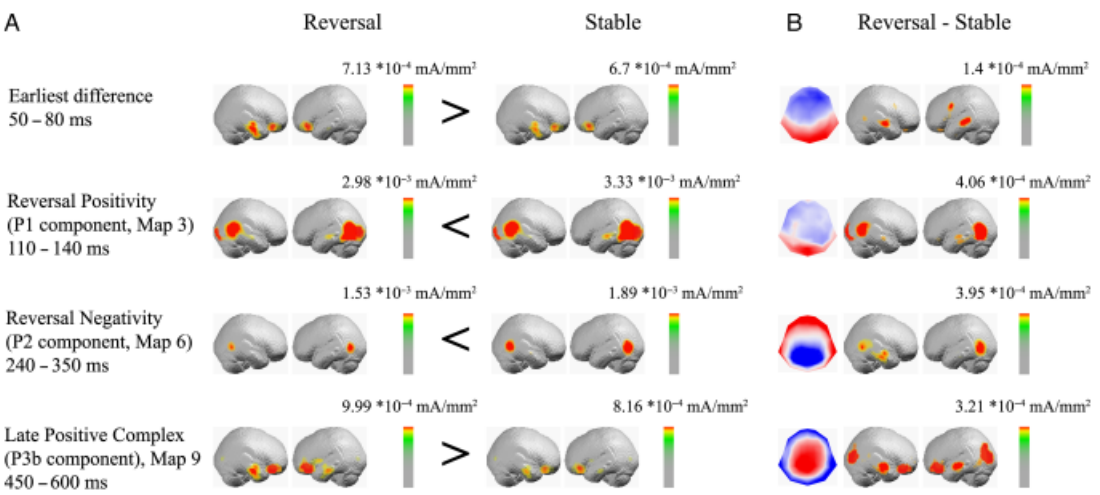

Figure 4. Sources of ERP amplitude differences. A: Current density for the reversal and stable conditions for the time periods of significant differences in ERP amplitudes and GFP. Colorbars indicate the maximum current density, and the arrow indicates the direction of the difference. B: Current density for the corresponding difference wave for the contrast reversal–stable.

ponent: It shows the same topography in the reversal and stable conditions, albeit with a higher GFP in the reversal than in the stable condition. Its concomitant source differences are stronger in the stable than in the reversal condition in early visual areas, including V1 and extrastriate cortex at around 130 ms. The intracranial currents in the reversal and stable conditions were also found in primary visual areas, albeit with a higher strength in the stable than in the reversal condition. Although the intracranial current estimation in the two conditions suggests stronger sources in the stable than in the reversal condition, the statistical comparison shows that the RP difference is the result of an increased strength of the same generator in the reversal than in the stable condition.

The RP component is preceded by an even earlier difference in both amplitude and field strength in the time window between 50 and 80 ms. Unlike for all other poststimulus differences, amplitudes in this time window are not different from baseline activity, which indicates that it does not reflect stimulus properties, but rather stimulus-independent intrinsic processes. The intracranial current differs in primary visual cortex during this period, but the statistical map of this comparison is different from the current density maps in the reversal and stable conditions and from that of the difference map. Moreover, the topographic maps in the reversal and stable conditions are different from the corresponding difference map; taken together, this suggests that it does not arise from a strength modulation of identical generators. Although some methodological traditions might discount this early difference as noise, it remains possible that this difference reflects endogenous changes in ongoing brain activity, especially under the current paradigm in which prestimulus EEG modulations have been identified (Britz et al., 2010). Clearly, further research is needed to address the exact nature of this early difference.

Reversal Negativity

The difference wave for the RN suggests an increased negativity in the reversal relative to the stable condition. The spatiotemporal ERP analysis, however, shows that it encompassed two ERP components: the N1 (Map 5) and the P2 (Map 6). Only the P2, but not the N1, differed with respect to GEV and GFP between the two conditions; both measures were increased in the stable relative to the reversal condition. This is corroborated by statistical comparisons of its concomitant intracranial sources, which revealed higher activity in the stable than in the reversal condition in lateral occipital and inferior temporal areas during the presence of the P2. No source differences were found during the presence of the N1 component. Moreover, the difference map during the P2 period has the same topography as the P2 in both conditions, whereas, during the N1 period, the difference map is different from the maps in the two conditions. The results from the surface and source space analysis suggest that the RN is an increased positivity in the stable condition. Because the comparison of two conditions can only give relative differences between these two conditions, this difference can likewise mean that activity in these areas is decreased during the perception of a reversal.

These results corroborate the findings from a previous study in which the intracranial generators for the RN were derived from difference waves and pointed toward sources in occipital-temporal and fusiform regions (Pitts et al., 2009). The intracranial currents in both conditions were found in the same areas, albeit with a higher strength in the stable than in the reversal condition. The distribution of the statistical map and the current density map were virtually identical, which indicates that the RN difference is the result of strength modulations of the same generator. The source of the difference wave was likewise found in virtually the same area. The location of this source difference is further in line with animal studies that suggest that the currently active percept of a binocular rivalry stimulus is reflected in discharge rates in these areas (Leopold & Logothetis, 1996; Logothetis et al., 1996; Sheinberg & Logothetis, 1997). Also, similar activity differences (less relative activity for reversals vs. stability) were found in these areas *preceding* perceptual reversals (Britz et al., 2010).

Overall, these results show that ventral stream activity is different for trials in which perception remains stable compared to trials in which perception switches, and this difference is the result of relatively greater activity during percept stabilization compared to perceptual reversal. Further work, however, is necessary to determine whether activity decreases for reversals or increases for stabilization.

Although the precise visual processes indexed by the RP and RN components remain unclear, the current analyses along with previous work (Britz et al., 2010) help to narrow the possibilities. The timing and neural generator locations of these two components suggest a tight correspondence with the implementation of the perceptual changes themselves. Whereas prestimulus activity in nonvisual parietal areas is associated with the initiation of reversals on upcoming trials and late-stage poststimulus activity (reflected by the LPC; see below) appears to reflect the cognitive appraisal of reversals, the RP and RN are situated at intermediate levels of processing that may actually carry out the perceptual transitions. Interestingly, the current analysis suggested that reversals are associated with increased activity during the RP time window ($\sim$ 130 ms) and decreased activity during the RN time window ($\sim$ 280 ms) relative to perceptual stability. One possibility is that activity in striate and extrastriate visual areas during the RP interval biases processing in inferior temporal areas during the subsequent RN interval, with the latter being most closely associated with the perceptual change itself. Alternatively, the RP might reflect the perceptual change, whereas the RN merely reflects a downstream consequence of this change (e.g., weaker activity for a less stable object representation). Further research may help determine the precise functional relationship between the processes reflected by these two components.

Late Positive Component

The LPC has been hypothesized to reflect the appraisal of perceptual reversals (Kornmeier & Bach, 2006) and it originates from a P3b-like topography in both conditions. The most prominent functional role of the P3b is voluntary target detection (here indicating the color of the percept), and it is, hence, elicited in each condition. Its topography is identical in both conditions, but its GEV and GFP are stronger in the reversal than in the stable condition. Its concomitant source differences were located in bilateral superior and middle temporal as well as left inferior frontal areas. Like for the RP and RN, very similar sources were found for the reversal and the stable conditions; that is, the current density maps and the statistical maps have the same distribution, which is again indicative of a strength modulation of the same underlying generators. This partly corroborates findings from a previous study that identified the neuronal generators for the LPC difference wave in anterior/inferior temporal regions (Pitts et al., 2009).

Summary and Conclusions

From the current study as well as previous studies, it appears as though visual brain areas (occipital and inferior temporal cortices) are responsible for implementing the perceptual changes that occur during bistable reversals whereas nonvisual brain areas in parietal cortex are involved in instigating these changes. Conversely, frontal and anterior temporal areas appear to be involved in the appraisal of reversals, for example, in evaluating what these perceptual changes mean for behavior. Moreover, the processes for the initiation, implementation, and appraisals of perceptual reversals are surprisingly independent from the physical aspects of the stimuli: They are highly similar for binocular rivalry and ambiguous figures.

References

Blake, R., & Logothetis, N. K. (2002). Visual competition. *Nature Reviews. Neuroscience*, *3*, 13–21. doi: 10.1038/nrn701.

Britz, J., Landis, T., & Michel, C. M. (2009). Right parietal brain activity precedes perceptual alternation of bistable stimuli. *Cerebral Cortex*, *19*, 55–65. doi: 10.1093/cercor/bhn056.

Britz, J., & Michel, C. M. (2010). Errors can be related to pre-stimulus differences in ERP topography and their concomitant sources. *NeuroImage*, *49*, 2774–2782. doi: 10.1016/j.neuroimage.2009.10.033.

Britz, J., Pitts, M. A., & Michel, C. M. (2010). Right parietal brain activity precedes the perceptual reversals during binocular rivalry. *Human Brain Mapping*. Advance online publication. doi: 10.1002/hbm.21117.

Brouwer, G. J., & van Ee, R. (2007). Visual cortex allows prediction of perceptual states during ambiguous structure-from-motion. *Journal of Neuroscience*, *27*, 1015–1023. doi: 10.1523/JNEUROSCI.4593-06.2007.

Gonzalez Andino, S. L., Michel, C. M., Thut, G., Landis, T., & Grave de Peralta, R. (2005). Prediction of response speed by anticipatory high-frequency (gamma band) oscillations in the human brain. *Human Brain Mapping*, *24*, 50–58. doi: 10.1002/hbm.20056.

Grave de Peralta Menendez, R., Murray, M. M., Michel, C. M., Martuzzi, R., & Gonzalez Andino, S. L. (2004). Electrical neuroimaging based on biophysical constraints. *NeuroImage*, *21*, 527–539. doi: 10.1016/j.neuroimage.2003.09.051.

Groening, K., Brodbeck, V., Moeller, F., Wolff, S., van Baalen, A., Michel, C. M., & Siniatchkin, M. (2009). Combination of EEG-fMRI and EEG source analysis improves interpretation of spike-associated activation networks in paediatric pharmacoresistant focal epilepsies. *NeuroImage*, *46*, 827–833. doi: 10.1016/j.neuroimage.2009.02.026.

Haynes, J.-D., & Rees, G. (2005). Predicting the stream of consciousness from activity in human visual cortex. *Current Biology*, *15*, 1301–1307. doi: 10.1016/j.cub.2005.06.026.

Haynes, J. D., Deichmann, R., & Rees, G. (2005). Eye-specific effects of binocular rivalry in the human lateral geniculate nucleus. *Nature*, *438*, 496–499. doi: 10.1038/nature04169.

Helmholtz, H. L. F. (1853). Über einige Gesetze der Vertheilung elektrischer Ströme in körperlichen Leitern mit Anwendung auf die thierisch-elektrischen Versuche. *Annalen der Physik und Chemie*, *9*, 221–233.

James, C. E., Britz, J., Vuilleumier, P., Hauert, C.-A., & Michel, C. M. (2008). Early neuronal responses in right limbic structures mediate harmony incongruity processing in musical experts. *NeuroImage*, *42*, 1597–1608. doi: 10.1016/j.neuroimage.2008.06.025.

Kornmeier, J., & Bach, M. (2004). Early neural activity in Necker-cube reversal: Evidence for low-level processing of a gestalt phenomenon. *Psychophysiology*, *41*, 1–8. doi: 10.1046/j.1469-8986.2003.00126.x.

Kornmeier, J., & Bach, M. (2005). The Necker cube—An ambiguous figure disambiguated in early visual processing. *Vision Research*, *45*, 955–960. doi: 10.1016/j.visres.2004.10.006.

Kornmeier, J., & Bach, M. (2006). Bistable perception—Along the processing chain from ambiguous visual input to a stable percept. *International Journal of Psychophysiology*, *62*, 345–349. doi: 10.1016/j.ijpsycho.2006.04.007.

Lantz, G., Michel, C. M., Pascual-Marqui, R. D., Spinelli, L., Seeck, M., Seri, S., & Rosen, I. (1997). Extracranial localization of intracranial interictal epileptiform activity using LORETA (low resolution electromagnetic tomography). *Electroencephalography and Clinical Neurophysiology*, *102*, 414–422. doi: 10.1016/S0921-884X(96)96551-0.

Lee, S. H., Blake, R., & Heeger, D. J. (2005). Traveling waves of activity in primary visual cortex during binocular rivalry. *Nature Neuroscience*, *8*, 22–23. doi: 10.1038/nn1365.

Lehky, S. (1995). Binocular rivalry is not chaotic. *Proceedings of the Royal Society of London, Series B: Biological Sciences*, *259*, 71–76. doi: 10.1098/rspb.1995.0011.

Lehmann, D., & Skrandies, W. (1980). Reference-free identification of components of checkerboard-evoked multichannel potential fields. *Electroencephalography and Clinical Neurophysiology*, *48*, 609–621. doi: 10.1016/0013-4694(80)90419-8.

Leopold, D. A., & Logothetis, N. K. (1996). Activity changes in early visual cortex reflect monkeys' percepts during binocular rivalry. *Nature*, *379*, 549–553. doi: 10.1038/379549a0.

Leopold, D. A., & Logothetis, N. K. (1999). Multistable phenomena: Changing views in perception. *Trends in Cognitive Sciences*, *3*, 254–264. doi: 10.1016/S1364-6613(99)01332-7.

Leopold, D. A., Wilke, M., Maier, A., & Logothetis, N. K. (2002). Stable perception of visually ambiguous patterns. *Nature Neuroscience*, *5*, 605–609. doi: 10.1038/nn0602-851.

Logothetis, N. K., Leopold, D. A., & Sheinberg, D. L. (1996). What is rivalling during binocular rivalry? *Nature*, *380*, 621–624. doi: 10.1038/380621a0.

Lumer, E. D., Friston, K. J., & Rees, G. (1998). Neural correlates of perceptual rivalry in the human brain. *Science*, *280*, 1930–1934. doi: 10.1126/science.280.5371.1930.

Lumer, E. D., & Rees, G. (1999). Covariation of activity in visual and prefrontal cortex associated with subjective visual perception. *Proceedings of the National Academy of Sciences, USA*, *96*, 1669–1673. doi: 10.1073/pnas.96.4.1669.

Meng, M., Remus, D. A., & Tong, F. (2005). Filling-in of visual phantoms in the human brain. *Nature Neuroscience*, *8*, 1248–1254. doi: 10.1038/nn1518.

Michel, C. M., de Peralta, R. G., Lantz, G., Gonzalez-Andino, S., Spinelli, L., Blanke, O., & Seeck, M. (1999). Spatiotemporal EEG analysis and distributed source estimation in presurgical epilepsy evaluation. *Journal of Clinical Neurophysiology*, *16*, 239–266. doi: 10.1097/00004691-199905000-00005.

Michel, C. M., Koenig, T., Brandeis, D., Gianotti, L., & Wackermann, J. (2009). *Electrical Neuroimaging*. Cambridge, UK: Cambridge University Press. doi: 10.1017/CBO9780511596889.

Michel, C. M., Murray, M. M., Lantz, G., Gonzalez, S., Spinelli, L., & Grave de Peralta, R. (2004). EEG source imaging. *Clinical Neurophysiology*, *115*, 2195–2222. doi: 10.1016/j.clinph.2004.06.001.

Murray, M. M., Brunet, D., & Michel, C. M. (2008). Topographic ERP analyses: A step-by-step tutorial review. *Brain Topography*, *20*, 249–264. doi: 10.1007/s10548-008-0054-5.

Pascual-Marqui, R. D., Michel, C. M., & Lehmann, D. (1994). Low resolution electromagnetic tomography: A new method for localizing electrical activity in the brain. *International Journal of Psychophysiology*, *18*, 49–65. doi: 10.1016/0167-8760(84)90014-X.

Pitts, M. A., Gavin, W. J., & Nerger, J. L. (2008). Early top-down influences on bistable perception revealed by event-related potentials. *Brain and Cognition*, *67*, 11–24. doi: 10.1016/j.bandc.2007.10.004.

Pitts, M. A., Martínez, A., Brewer, J. B., & Hillyard, S. A. (2010a). Early stages of figure–ground perception: ERPs and the face–vase illusion. *Journal of Cognitive Neuroscience*, *23*, 1–16. doi: 10.1162/jocn.2010.21438.

Pitts, M. A., Martínez, A., & Hillyard, S. A. (2010b). When and where is binocular rivalry resolved in the visual cortex? *Journal of Vision*, *10*, 25. doi: 10.1167/10.14.25.

Pitts, M. A., Martínez, A., Stalmaster, C., Nerger, J. L., & Hillyard, S. A. (2009). Neural generators of ERPs linked with Necker cube reversals. *Psychophysiology*, *46*, 694–702. doi: 10.1111/j.1469-8986.2009.00822.x.

Pitts, M. A., Nerger, J. L., & Davis, T. J. R. (2007). Electrophysiological correlates of perceptual reversals for three different types of multistable images. *Journal of Vision*, *7*, 1–14.

Plomp, G., Michel, C. M., & Herzog, M. H. (2010). Electrical source dynamics in three functional localizer paradigms. *NeuroImage*, *53*, 257–267. doi: 10.1016/j.neuroimage.2010.06.037.

Polonsky, A., Blake, R., Braun, J., & Heeger, D. J. (2000). Neuronal activity in human primary visual cortex correlates with perception during binocular rivalry. *Nature Neuroscience*, *3*, 1153–1159.

Schulz, E., Maurer, U., van der Mark, S., Bucher, K., Brem, S., Martin, E., & Brandeis, D. (2008). Impaired semantic processing during sentence reading in children with dyslexia: Combined fMRI and ERP evidence. *NeuroImage*, *41*, 153–168. doi: 10.1016/j.neuroimage.2008.02.012.

Sheinberg, D. L., & Logothetis, N. K. (1997). The role of temporal cortical areas in perceptual organization. *Proceedings of the National Academy of Sciences, USA*, *94*, 3408–3413. doi: 10.1073/pnas.94.7.3408.

Sperli, F., Spinelli, L., Seeck, M., Kurian, M., Michel, C. M., & Lantz, G. (2006). EEG source imaging in pediatric epilepsy surgery: A new perspective in presurgical workup. *Epilepsia*, *47*, 981–990. doi: 10.1111/j.1528-1167.2006.00550.x.

Spinelli, L., Gonzalez Andino, S., Lantz, G., Seeck, M., & Michel, C. M. (2000). Electromagnetic inverse solutions in anatomically constrained spherical head models. *Brain Topography*, *13*, 115–125. doi: 10.1023/A:1026607118642.

Sterzer, P., & Kleinschmidt, A. (2007). A neural basis for inference in perceptual ambiguity. *Proceedings of the National Academy of Sciences, USA*, *104*, 323–328. doi: 10.1073/pnas.0609006104.

Sterzer, P., Kleinschmidt, A., & Rees, G. (2009). The neural bases of multistable perception. *Trends in Cognitive Sciences*, *13*, 310–318. doi: 10.1016/j.tics.2009.04.006.

Sterzer, P., & Rees, G. (2008). A neural basis for percept stabilization in binocular rivalry. *Journal of Cognitive Neuroscience*, *20*, 389–399. doi: 10.1162/jocn.2008.20039.

Sterzer, P., Russ, M. O., Preibisch, C., & Kleinschmidt, A. (2002). Neural correlates of spontaneous direction reversals in ambiguous apparent visual motion. *NeuroImage*, *15*, 908–916. doi: 10.1006/nimg.2001.1030.

Tong, F., Meng, M., & Blake, R. (2006). Neural bases of binocular rivalry. *Trends in Cognitive Sciences*, *10*, 502–511. doi: 10.1016/j.tics.2006.09.003.

Tong, F., Nakayama, K., Vaughan, J. T., & Kanwisher, N. (1998). Binocular rivalry and visual awareness in human extrastriate cortex. *Neuron*, *21*, 753–759. doi: 10.1016/S0896-6273(00)80592-9.

Vaughan, H. G. J. (1982). The neural origins of human event-related potentials. *Annals of the New York Academy of Sciences*, *388*, 125–138. doi: 10.1111/j.1749-6632.1982.tb50788.x.

Vulliemoz, S., Rodionov, R., Carmichael, D. W., Thornton, R., Guye, M., Lhatoo, S. D., & Lemieux, L. (2010). Continuous EEG source imaging enhances analysis of EEG-fMRI in focal epilepsy. *NeuroImage*, *49*, 3219–3229. doi: 10.1016/j.neuroimage.2009.11.055.

Wolfe, J. M. (1983). Influence of spatial frequency, luminance, and duration on binocular rivalry and abnormal fusion of briefly presented dichoptic stimuli. *Perception*, *12*, 447–456. doi: 10.1068/p120447.

Wunderlich, K., Schneider, K. A., & Kastner, S. (2005). Neural correlates of binocular rivalry in the human lateral geniculate nucleus. *Nature Neuroscience*, *8*, 1595–1602. doi: 10.1038/nn1554.

Zumsteg, D., Friedman, A., Wieser, H. G., & Wennberg, R. A. (2006). Propagation of interictal discharges in temporal lobe epilepsy: Correlation of spatiotemporal mapping with intracranial foramen ovale electrode recordings. *Clinical Neurophysiology*, *117*, 2615–2626. doi: 10.1016/j.clinph.2006.07.319.

Supporting Information

Additional supporting information may be found in the online version of this article:

Figure S1: Baseline-corrected exemplar ERP waveforms.

Figure S2: Periods of significant differences of ERP amplitudes from baseline.

Please note: Wiley-Blackwell are not responsible for the content or functionality of any supporting materials supplied by the authors. Any queries (other than missing material) should be directed to the corresponding author for the article.

(Received February 2, 2011; Accepted April 16, 2011)